



Behavior of cantilever secant pile wall supporting excavation in sandy soil considering pile-pile interaction

Mohamed I Ramadan^{1,2} · Mohamed Meguid³

Received: 30 July 2019 / Accepted: 25 May 2020 / Published online: 13 June 2020
© Saudi Society for Geosciences 2020

Abstract

This study presents the results of a numerical investigation performed to investigate the behavior of a cantilever secant pile wall (CSPW) used to support excavation in sandy soil. These types of excavations have the potential to cause severe ground movement and possible damage to the adjacent structures. A major concern in supporting excavation is to predict and control ground movement associated with excavation particularly in cohesionless soils, as it could trigger global instability and catastrophic failure. The magnitude and distribution of lateral earth pressure and ground movement depend mainly on soil properties, excavation depth, excavation plan geometry, the stiffness of the supporting wall, and the contact between the secant piles themselves. Three-dimensional finite element model has been developed in this study to capture the excavation and wall geometry. A parametric study has been performed using a wide range of sand density, excavation depth, wall flexural stiffness, and bonding between piles within the wall. The results allowed for the development of an approach to predict both the wall deflection for the case of fully and partially bonded piles. This will help engineers to predict ground movement and select an appropriate supporting system that can maintain the stability of the adjacent structures.

Keywords Numerical modeling · Cantilever wall · Excavation support · Secant piles · Pile-pile interface

Introduction

Ground movement induced by excavation is a challenging problem in geotechnical engineering. Deep excavation in granular material can cause severe ground movement and subsequent damage to the adjacent structures. Most of the previous studies have focused on examining ground movement induced by deep excavation in clay, with emphasis on soft clay material (e.g., Ou et al. 1993; Wong et al. 2002;

Ge 2002; Hu et al. 2003; Liu et al. 2005; Finno et al. 2006; Kung et al. 2007; Liu et al. 2011; Tan and Wei 2011; Ng et al. 2012; and Liu et al. 2018). However, studies related to excavation in sandy soil are limited to few case histories (Hsiung 2009; Khoiri and Ou 2013; Nikolinakou et al. 2011; Li and Lehane 2010; Zahmatkesh and Choobasti 2015; Hsiung et al. 2016; Sert et al. 2016; Ji et al. 2019). Several case histories have been analyzed by Moormann (2004), and the results showed that for non-cohesive soil the average value of the normalized horizontal deflection ($\delta_{h-max}/H\%$) and vertical displacement at the ground surface ($\delta_{v-max}/H\%$) are about 0.25% and 0.33%, respectively. Such values are small when compared to soft clay where $\delta_{h-max}/H\% > 1\%$ and $\delta_{v-max}/H\%$ has an average value of 1%. These relatively small ground movements are considered significant for sandy soil, which could lead to the full mobilization of strength and cause failure. Rowe and Peaker (1965) and Bica and Clayton (2004) performed a series of physical model tests and concluded that theoretical passive earth pressure coefficients based on soil peak friction angle values were unsafe as reported by Milligan et al. (2008). In loose sand, full theoretical pressure is reached after a large wall movement. However, in dense

Responsible Editor: Zeynal Abiddin Erguler

✉ Mohamed I Ramadan
mohamedih@mun.ca; mohamed1@aun.edu.eg

Mohamed Meguid
mohamed.meguid@mcgill.ca

- ¹ Faculty of Engineering-Rabigh, King Abdulaziz University, Jeddah, Saudi Arabia
- ² Civil Engineering Department, Faculty of Engineering, Assiut University, Assiut, Egypt
- ³ Civil Engineering and Applied Mechanics, McGill University, Montreal, Canada

sand, progressive soil failure occurs at an average soil strength less than the peak value.

Limit equilibrium method had been used to design cantilever embedded wall in sand (Burland et al. 1981; Bolton and Powrie 1987; Bica and Clayton 1989; Bolton et al. 1989, 1990; Madabhushi and Chandrasekaran 2005; Conte et al. 2013, 2015). It is assumed that there is a pivot point close to wall tip around which the wall rotates rigidly. Active earth pressure is assumed above the pivot point on the retained side while passive earth pressure below that point on the excavated side. An alternative method had been proposed by King (1995) based on a series of centrifuge tests. He suggested that the location of the pivot point is at 0.35 times the embedded depth of the wall. Later, Day (2001) suggested that the location of the pivot point is not constant and its location is a function of the ratio of passive to active earth pressure coefficient. Conte et al. (2017) proposed an analytical method to predict the net earth pressure on the wall and bending moment of the wall. Their proposed method was in a good agreement with other results (King 1995; Conte et al. 2013) and experimental results (Madabhushi and Zeng 2006). It should be noted that such theoretical methods based on the rotation of a rigid wall may not be suitable for relatively flexible embedded walls where the passive earth pressure is partially mobilized (Gaudin et al. 2004). Mei et al. (2009) developed a model that can predict earth pressure as a function of wall movement. Such solution helps in the design of embedded retaining walls where the full active or passive pressures did not reach.

Hsiung (2009); Khoiri and Ou (2013); Nikolinakou et al. (2011); Li and Lehane (2010); Zahmatkesh and Choobbasti (2015); and Hsiung et al. (2016) performed finite element modeling (FEM) for excavation in sand. The FEM was calibrated using several case studies. The measured lateral movements indicate that the wall initially behaved as a cantilever; however, after the installation of the struts, the wall started to behave as a propped cantilever and the movements continued to increase during the excavation (Hsiung 2009). Khoiri and Ou (2013) recommended that a suitable value of unloading-reloading elastic modulus (E_{ur}^{ref}) should be used to capture the small-strain behavior at the excavation base. In other analysis model input, parameters were calibrated through laboratory compression and triaxial shear tests on sand specimens obtained from the excavation site (Nikolinakou et al. 2011). They concluded that good predictions of excavation performance can be achieved through careful site-specific calibration of the sand behavior and using a constitutive model capable of representing variations in stress-strain-strength properties as function of the confining stress and void ratio. Hsiung et al.

(2016) indicated that the use of Mohr-Coulomb model with soil modulus obtained from in situ dilatometers for loose to medium dense sands yields reasonable predictions of the excavation-induced wall displacements. For an excavation in sand, the wall initially behaves in cantilever mode and then changes to prop mode after the struts are installed.

In the above studies, the numerical analyses were well validated using site investigation or laboratory testing programs such that model parameters were well-calibrated and the soil model was identified clearly. The challenge in most numerical studies was to select an appropriate constitutive model and the needed soil parameters. These studies concluded that soil stiffness generally controls the ground movements induced by excavation. However, there is a need for an extensive parametric study that provides prediction of ground movement induced by excavation in sand over a wide range of parameters, such as soil stiffness, wall stiffness, interaction between piles in the wall, and excavation depth.

Long (2001) carried out 36 deep excavation cases analysis for soft soil over laying stiff soil. He concluded that the excessive movements $\delta_{h-max}/H > 0.3\%$ were occurred due to the presence of a cantilever stage at the beginning of an excavation sequence. At the cantilever stage, the lateral deflection at the top of the wall is almost equal to that at the final stage (Hashash 1992). This means that the initial cantilever deflection at the top of the wall mainly contributes to the final wall movement, especially for the final wall deflection near the ground surface (Clough and O'Rourke 1990). This means that a main cause of excessive ground movements can also be the over-excavation in the initial excavation stage. In some cases (Long 2001; and Osouli and Hashash 2010), the installed anchors or struts may not be stiff enough to control the deformation and the final lateral deflection and ground surface will be similar to the cantilever stage case.

In design and analytical models, secant pile walls (SPW) are commonly simplified as an equivalent continuous wall (Altuntas et al. 2009; and Finno et al. 2002). The interface between secant piles are considered to be fully bonded. A few field tests have been conducted on secant pile walls (Finno et al. 2002; Finno and Bryson 2002; Mohamad et al. 2011). Secant pile walls have only been tested in laboratory by Liao et al. (2014). From these mentioned studies, it was observed that after excavation a reduction in wall stiffness was observed. Liao et al. (2014) concluded that the early strength of primary piles, the time intervals of bonding (TIB), and the effects of bonding quality could be a source of such wall stiffness reduction. They carried out an extensive experimental study to examine the interface and the interaction between secant piles under tension, shear, and bending tests. They found that poor bonding quality will cause cracking or local failure on the secant face, so reduce the overall strength of secant pile walls.

Scope and objectives

In the present study, excavation depths of up to 6 m are considered. Although this represents a case of shallow excavation, the results can be applied for the analysis of initial cantilever stage of deep excavations before the installation of first level struts/anchors. The effect of relative density of the sand is evaluated by considering range of parameters that reflect medium as well as dense sand material. The study is further extended to examine the uncertainties that may exist in the construction of SPWs. In addition, the role of interface condition between piles is examined.

Numerical model

Cantilever secant pile wall (CSPW) supporting excavation in sandy soil was conducted using PLAXIS 3D finite element software (2006). The model geometry, mesh properties, soil parameters, dimensions and properties of CSPW are presented. No ground water level was assumed in this study.

Geometry and meshing

The finite element (FE) model geometry was selected so that the boundaries are far enough to affect the response of the system, particularly near the supporting wall as suggested by Ramadan et al. (2018). Several excavation dimensions were investigated. However, excavation width (B) of 10 m and wall width (W) of 10 m were selected in the parametric study. While the model dimensions were chosen to be 50×50 m. The FE model is shown in Fig. 1. Only one side of the excavation was supported using CSPW. The other three sides were restrained from lateral movement towards the excavation. The excavation geometry is based on that reported by Turner et al. (2004) where only one side of the excavation requires support using pile wall to prevent failure of nearby structures. The other three sides were assumed to be as sloped or supported by other wall types that are not connected to the investigated pile wall. This assumption can also be valid for the cases of excavation by section which is used for large foundation pits without horizontal struts (Nie 2019). Although in some cases all pile heads may be connected to a guide beam of plain concrete or cement-bentonite mixture for construction purpose, such beam is not rigid enough to control the deflection of piles in the cantilever wall. In the present study, it was considered that pile heads are free.

In a typical three-dimensional analysis, the mesh density within the excavation can affect the accuracy of the analysis (Ou et al. 2010). For the current model, the mesh was refined near the piles where the stresses are expected to be high. A coarser mesh was used outside the area of interest where the stresses are generally low, as shown in Fig. 1. The distance

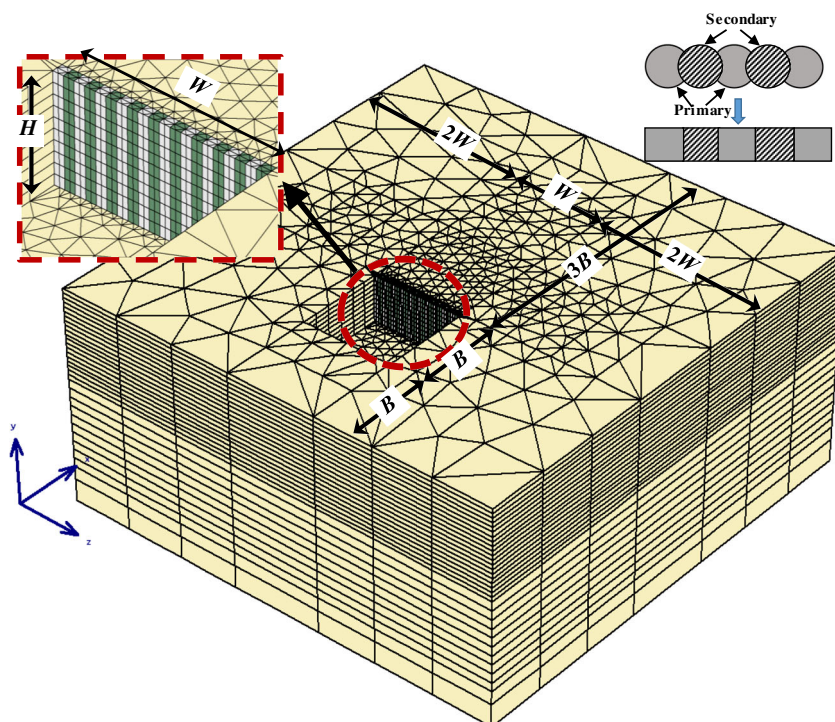
between the horizontal work planes (i.e., in y -direction) can also affect the accuracy of the results. Therefore, the distance between these planes was taken as 0.5 m from the ground surface up to 10 m depth and increased to 1.0 m towards the bottom of the model. A preliminary analysis confirmed that soil movement due to excavation does not extend beyond 10 m depth into the sandy soil. The model boundaries were selected to be far enough from the excavation zone so that not causing strain localization, as shown in Fig. 1. All vertical boundary conditions of the model sides were considered to restrict perpendicular horizontal movement while allow vertical movement. The boundary condition of the model base was set as fixed in all directions.

The importance of using 3D model rather than plane strain (PS) analysis was discussed by Hsiung et al. (2016). They found that PS model overestimates soil deformations by about 40% for a wide range of pile wall width (W) to excavation width (B) ratios. To investigate the effect of excavation geometry in the present study, full 3D analysis is, therefore, needed. In addition, using the 3D model will allow for the effect of individual pile stiffness (soft/firm–hard piles) within the secant wall to be investigated. Moreover, examining the effect of pile–pile interaction in the secant wall becomes feasible when the interacting pile are fully simulated.

Soil model

Uniform sandy soil was considered in the FEM analysis. Four different relative densities D_r (50%, 60%, 70%, and 80%) were considered in the analysis ranging from dense to medium sand. Soil material was modeled using the hardening soil model (HSM). The HSM adopts a hyperbolic stress–strain representation for the soil and implements three Young's moduli; E_{50}^{ref} , $E_{\text{oed}}^{\text{ref}}$, $E_{\text{ur}}^{\text{ref}}$, defined as the secant, odometer, and unloading-reloading elastic modulus at the reference pressure p^{ref} , respectively. The moduli at the in situ stress state are automatically computed as a function of the current stress state. The sand parameters at different relative densities were calculated using the empirical method suggested by Brinkgreve et al. (2010) to derive model parameters for sand material. They used regression analysis on a collection of soil data (general soil data, triaxial tests, and oedometer tests) from Jefferies and Been (2006) and others. The empirical equation of Brinkgreve et al. (2010) has been widely used to model sandy soil using the HSM model (Knappett et al. 2016; Sert et al. 2016; Gazetas et al. 2016; Martinkus et al. 2017; Panagoulas et al. 2018; Achmus et al. 2019). The parameters used in the present study are shown in Table 1. Fifteen-node triangular elements were used to model the soil. Soil-pile and pile-pile interaction were simulated using interface elements. Interface elements are zero length elements of pairs of nodes which are numerically integrated using 6 points Gauss

Fig. 1 Finite element model: mesh and geometry



integration. Each node has three translation degrees of freedom. Such element allows for differential displacements between the node pairs as slipping and gapping.

Excavation support system

The secant pile wall was modeled to represent a series of concrete piles with a diameter of 500 mm. Square piles were considered in the analysis to simplify the simulation process as shown in Fig. 1 as recommended by Bryson and Medina (2010). SPW was modeled as linear elastic material with properties that represent concrete material as shown in Table 2. The flexural stiffness used in the analysis was for cracked section reduced by 30% as recommended by Ou (2006). Coulomb friction model was used to simulate the interface

behavior. Soil-wall interaction was assumed to behave as rough interaction with interface friction coefficient $\mu = 1$ as recommended by Bryson and Medina (2010) and Ng et al. (2015).

Model validation

The numerical model has been validated using Gaudin et al. (2004) experimental centrifuge test results. Other available centrifuge test results of embedded cantilever wall in sand can be used to validate the numerical model. However, centrifuge tests in literature (Zhu and Yi 1988; and King and McLoughlin 1993) simulated excavation by stopping the centrifuge and re-spinning up it to the required acceleration. With such very simple technique,

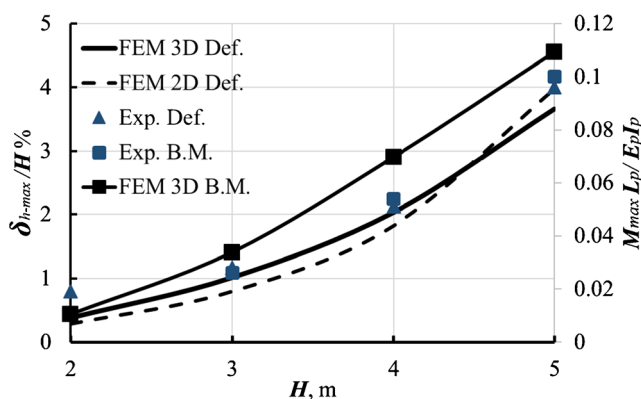
Table 1 Soil parameters in finite element model

Parameter	Input
Soil unit weight, γ (kN/m ³)	$15 + (4 D_r\% / 100)$
Secant elastic modulus, E_{50}^{ref} (kN/m ²)	$600 \times D_r\%$
Odometer elastic modulus, E_{oed}^{ref} (kN/m ²)	E_{50}^{ref}
Unloading-reloading elastic modulus, E_{ur}^{ref} (kN/m ²)	$3 E_{50}^{ref}$
The rate of stress dependency, m	$0.7 - (D_r\% / 320)$
Angle of internal friction, ϕ' (°)	$28 + (12.5 \times D_r\% / 100)$
Dilation Angle, ψ' (°)	$-2 + (12.5 \times D_r\% / 100)$
Failure ratio, R_f	$1 - (D_r\% / 800)$
Interface friction coefficient, μ	1

Table 2 Pile parameters in finite element model

Pile type	Input parameter	
	Elastic modulus, E_p (kN/m ²)	Poisson's ratio, ν
Hard (RC) pile	2.1×10^7	0.2
Firm (PC) pile	1.2×10^7	0.2
Soft (CB) pile	0.6×10^7	0.2

the real stress state and the main wall displacements could not be simulated correctly (Gaudin et al. 2004). Gaudin et al. (2004) performed a series of centrifuge tests using a robot to simulate the excavation process in-flight. An aluminum plate was used as a wall embedded in a sand of relative density of about 70%. The embedded full length of the wall was 10 m in prototype scale. The wall had a flexural stiffness of about 6.5 MN m² in prototype scale. Excavation was carried out at 50 g of acceleration. Wall displacement and bending moment profile was obtained using strain gauges mounted on both sides of the wall. The numerical model of the present study was validated using the results of Gaudin et al. (2004) in terms of maximum top wall displacement and maximum bending moment. Numerical model geometry was the same as discussed in the previous section. Soil parameters have been calculated corresponding to $D_r = 70\%$ according to Brinkgreve et al. (2010), as shown in Table 1. In the validation of the numerical model, the interaction between piles in the wall was considered as rough or fully bonded, so that the wall behaves as a continuous wall similar to the centrifuge test. Wall flexural stiffness has been considered in the FEM so that both the physical and the numerical models have the same flexural stiffness per meter length of the wall. Soil-wall interface friction coefficient has been taken as 0.5 as recommended by Hikooei (2013) and Kenny and Jukes (2015). Figure (2) presents the maximum lateral deflection at the top of the wall

**Fig. 2** Numerical model validation with experimental results

versus the excavation depth (H). Results show a good agreement between the measured and calculated response. In addition, the normalized maximum bending moment is presented in Fig. 2 versus the excavation depth (H). Moment values agreed well with the results reported by Gaudin et al. (2004).

A two-dimensional plane strain FE model of the same problem of Gaudin et al. (2004) was established. Solid elements were used for both soil and wall. Zdravkovic et al. (2005), Dong et al. (2012), and Dong et al. (2014) reported that shell elements in 3D FEM (or beam elements in 2D FEM) produce larger wall deflection and ground movement compared to solid elements. Similar conclusion was observed during the current analysis. Figure 2 shows that results of both 2D and 3D FEM are in a good agreement with the experimental results by Gaudin et al. (2004). It should be noted that friction angle and dilation angle in 2D FEM were increased by 10% for plane strain conditions from 3D FEM case as recommended by Bolton (1986). It can be concluded that 3D FEM of the wall in the present study behaves similar to plane strain conditions. This means that the boundary conditions and geometry of the 3D wall will not affect the results in terms of maximum lateral deflection or maximum bending moment of the wall.

Parametric study

Different parameters have been examined in the present study. Relative sand densities D_r of 50%, 60%, 70%, and 80% have been considered. In addition, the effect of excavation geometry has been examined. The SPW resists soil pressure by mobilizing flexural stiffness, which can be controlled by changing the pile diameter, pile length, or pile material. There are different types of SPW system, namely, hard-hard secant pile wall (H-H SPW), hard-firm secant pile wall (H-F SPW), and hard-soft secant pile wall (H-S SPW). H-H SPW is constructed of a primary (drilled first) reinforced concrete pile (RCP) and a secondary RCP. H-F SPW is constructed of a primary plain concrete pile (PCP) and a secondary RCP. H-S SPW is constructed of cement-bentonite pile (CBP) as a primary pile and RCP as a secondary pile. A sketch of the secant pile profile showing the primary and secondary piles is shown in Fig. 1. The overlapping between piles is about up to 30% of the pile diameter. As discussed earlier, the TIB is an important parameter that can cause significant reduction in wall stiffness. In the present study, the effect of TIB has been considered using interface elements introduced between piles. Where fully bonded piles have interface coefficient $\mu = 1$, while $\mu = 0$ is used for piles with no bonding (e.g., tangent piles).

Results of parametric study

Effects of sand relative density

Sand relative densities of 50, 60, 70, and 80% have been examined using the developed model. These values cover a wide range of medium to dense sand. As the pile wall behaves as a cantilever, the maximum lateral wall deflection (δ_{h-max}) is expected at the top of the wall as shown in Fig. 3. Maximum shear force (Q_{max}) is at the excavation level. However, the maximum bending moment (M_{max}) is almost at 1 m below of the base of the excavation. It was found from the results that the increase in sand density significantly decrease the lateral deflection of the wall (δ_h), shear force (Q), bending moment (M), and surface settlement (δ_v) as shown in Figs. 3 and 4. The change in sand density usually corresponds to change in soil stiffness. As the soil stiffness increases, soil movement decreases. Figure 5 summarizes the results for the cases of pile wall length of 20 m. As the relative density increases $\delta_{h-max}/H\%$ decreases. At medium relative density of 50%, $\delta_{h-max}/H\%$ ranges between 0.1 and 0.4% for H ranges between 3 and 6 m. As relative density increases to 80%, $\delta_{h-max}/H\%$ decreases to 0.05% and 0.25% for H of 3 m and 6 m, respectively as shown in Fig. 5. Similar observations were found for $\delta_{v-max}/H\%$.

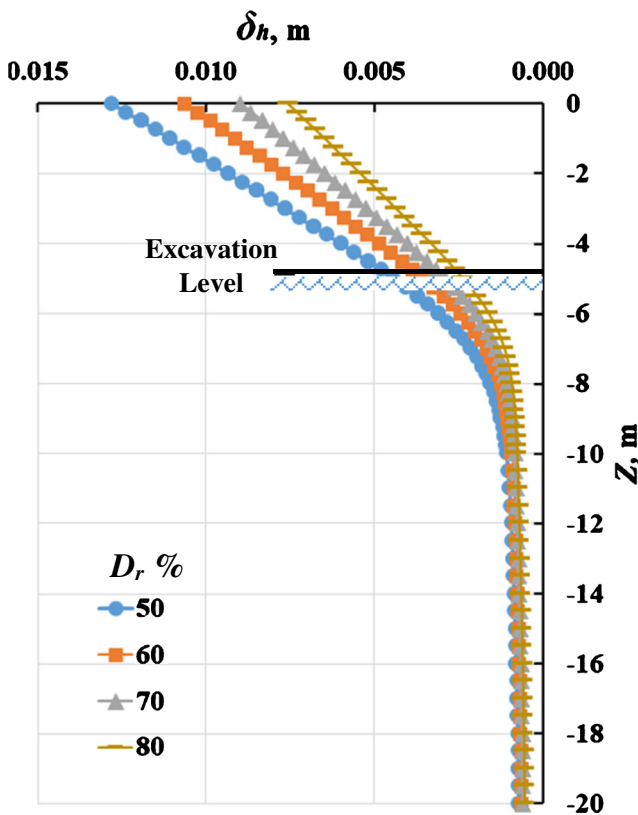


Fig. 3 Lateral deflection profile of middle pile at different D_r ($H = 5$ m and $L = 20$ m)

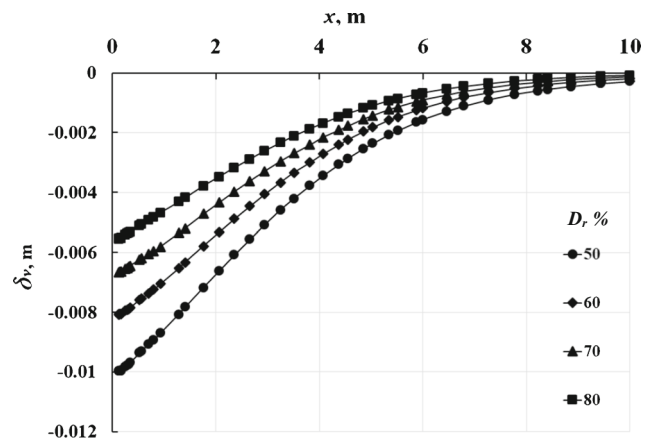


Fig. 4 Vertical ground surface displacement at different D_r ($H = 5$ m and $L = 20$ m)

Effect of excavation depth

Figure 5 shows the relationship between soil movement as $\delta_{h-max}/H\%$ and excavation depth (H). At very shallow excavation depth ($H = 1$ m), δ_{h-max} can be considered very small (less than 2 mm) which is not significant. However, as H increases δ_{h-max} increases. The rate of increase becomes rapid at $H = 3$ m. The maximum surface settlement (δ_{v-max}) is found to be also small up to $H = 2$ m. For excavation depth more than 2 m, δ_{v-max} increases at a high rate for $H > 3$ m. This behavior is found for all investigated cases of relative density.

Effect of Wall Length

The effect of wall length (L) has been examined for four different pile lengths, namely 10, 12, 14, and 20 m. It was found that δ_h is almost the same for all lengths except $L = 10$ m where the pile wall displayed rigid response while other cases the wall displayed flexible responds. The same conclusion can be made for δ_v . More details regarding pile flexibility will be discussed later.

Effect of wall flexural stiffness

Wall flexural stiffness ($E_p I_p$) is known to play an important role in controlling the response of cantilever pile wall in

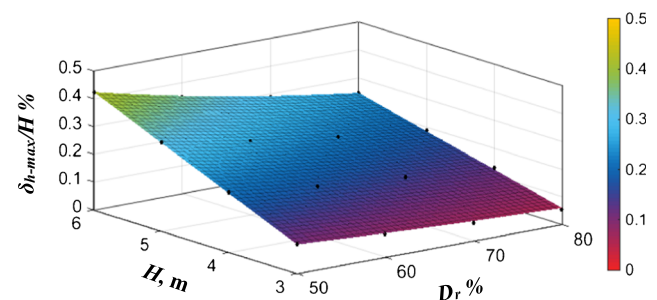


Fig. 5 Variation of $\delta_{h-max}/H\%$ at nifferent H and D_r ($L = 20$ m)

response to excavation. The use of secant pile wall to support excavation in sand in the presence of water is critical. Insufficient overlap between the piles due to difference in pile verticality will cause leakage allowing sand water mixture to flow into the excavation causing instability and possibly failure. Pile walls constructed of primary CBPs have a certain amount of plasticity after hardening making it more suitable for watertight walls that allows for the installation of a secondary reinforced concrete piles (Korff et al. 2007; and Gannon 2016). In the present study, three cases of wall stiffness are examined: hard–hard secant pile wall (H-H SPW), hard–firm secant pile wall (H-F SPW), and hard–soft secant pile Wall (H-S SPW). A summary of the elasticity modulus values used for different pile materials is shown in Table 2 according to Ou et al. (2010). However, it should be noted that as the current study considers dry sand condition, so the effect of water flow or leakage presence as discussed earlier is out of the scope of the present study. Figure 6 shows that the increase in $E_p I_p$ results in a decrease in pile wall deflection, particularly above the excavation depth. However, below the excavation depth all investigated cases presented almost the same deflection profile. No significant effect for $E_p I_p$ on the maximum pile wall deflection was found up to $H = 2$ m. At $H = 3$ m, the change in stiffness started to influence the response, which gradually increased with the increase in H . The complete profile of $\delta_w/H\%$ along the wall width is shown in Fig. 6. It is found that the increase in wall deflection due to the decrease of $E_p I_p$ extends across the width of the wall. The same observation was found for pile wall lengths of 10 and 20 m, which corresponds to rigid and flexible wall, respectively. For the HH case, $\delta_w/H\%$ at the top for $L = 20$ m is less than that for $L = 10$ m. The shorter pile behaves as a rigid pile that rotates around a point on its vertical axis. By increasing pile rigidity and decreasing pile length, the point of rotation moves down

and the pile top deflection increases. However, as $E_p I_p$ decreases, $\delta_w/H\%$ of the 10-m wall decreases slightly and approach that of the 20-m wall for HF or HS cases, respectively. This means that the flexural stiffness factor $E_p I_p/L$ controls the flexibility of the wall. However, for the range of wall lengths used in the current study (10, 12, 14, and 20 m), which represents a typical range for cantilever pile walls, no significant difference in response was calculated. When $E_p I_p$ changes, such effect appears. Figure 7 shows the maximum normalized bending moment, $M_{max} L_p / E_p I_p$, different cases of HS, HF, and HH for $\mu = 1$. It can be observed that $M_{max} L_p / E_p I_p$ increases as pile wall flexural stiffness ($E_p I_p$) decreases. It is important to be aware that hard piles in HS or HF cases must be designed to sustain that increase in bending moment otherwise the system will fail. It is also important to check that soft or firm piles will be able to sustain the developed bending moment otherwise cracks will occur and may cause leakage in case of high ground water table resulting in strength reduction and failure of the excavation supporting system.

Effect of bonding between piles

The time intervals of bonding (TIB) during installation is known to affect the bonding strength between piles. At the time of secondary piles installation, the concrete of the primary piles may be either too hard or too soft. A “perfect” age of the primary columns when installing the secondary ones is difficult to be achieved (Korff et al. 2007; and Gannon 2016). If the concrete is too hard, irregularities or cracks will usually develop. If it is too soft, deformation of the primary piles will occur and the bonding between piles will be weak. In the current study, interface elements following Coulomb friction model are introduced between piles to simulate the bonding condition. The friction coefficient, μ , ranges between

Fig. 6 Normalized lateral deflection at the top of the wall along wall width at different wall flexural stiffness ($E_p I_p$) and different bonding between piles ($D_r = 70\%$, $H = 5$ m, and $L = 20$ m)

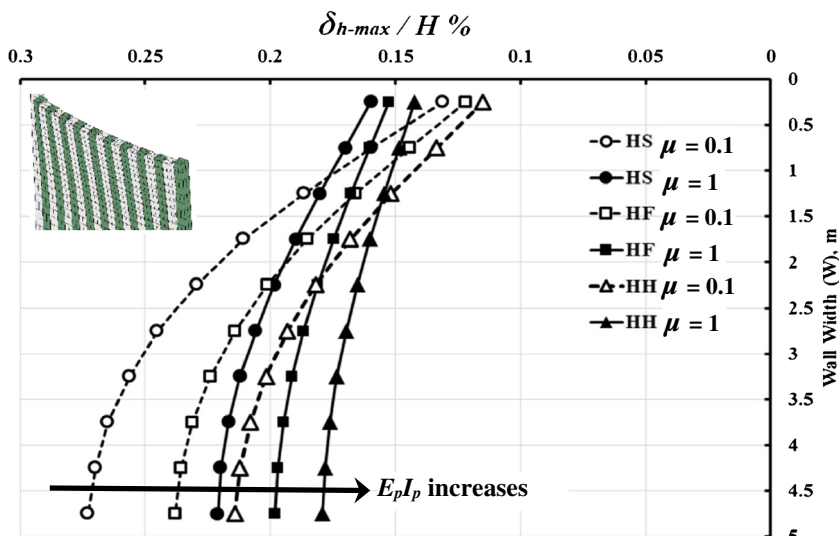
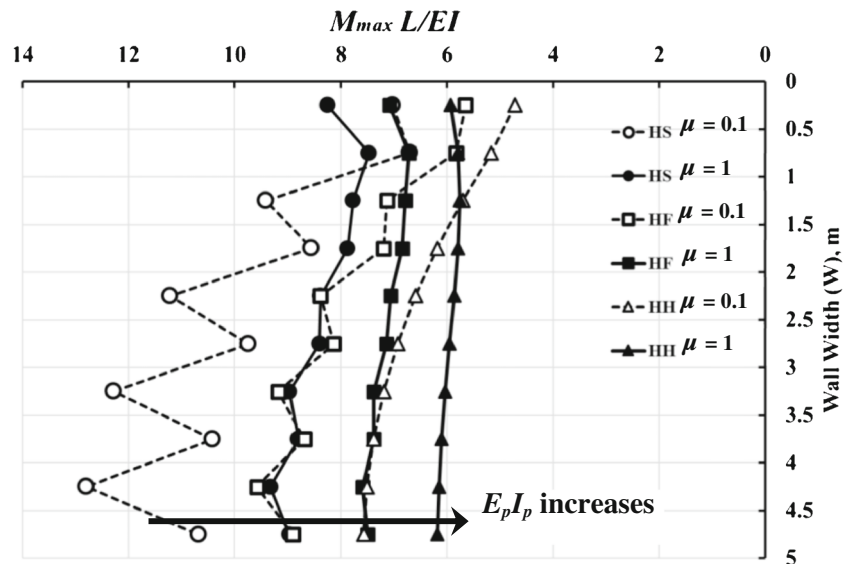


Fig. 7 Normalized maximum bending moment along wall width at different wall flexural stiffness ($E_p I_p$) ($D_r = 70\%$, $H = 5$ m, and $L = 20$ m)



“0” for piles of no bonding (similar to tangent piles) and “1” for piles of perfect bonding. Different values of μ have been examined in this section.

It was found from the results that both $\delta_{h-max} H\%$ and $\delta_{v-max}/H\%$ increase rapidly by increasing H for $\mu = 0$. The deviation between different μ values becomes significant for $H \geq 3$ m. As μ increases the rate of change in $\delta_{h-max}/H\%$ (or $\delta_{v-max}/H\%$) decreases. Figure 8 shows such variation in terms of $\delta_{h-fric} \%$ (the same behavior was found for $\delta_{v-fric} \%$) versus μ for different H values, where

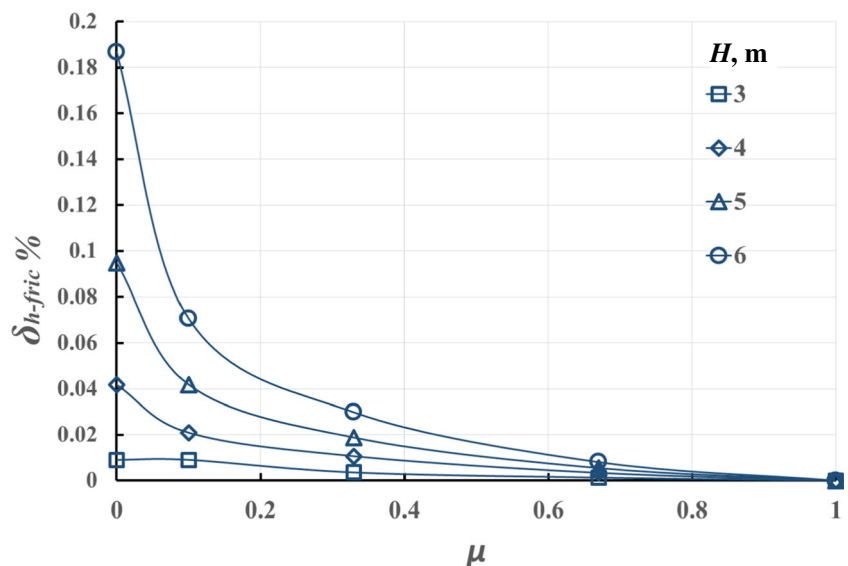
$$\delta_{h-fric} \% = (\delta_{h-max}/H) \%_{(for\ any\ \mu\ value)} - (\delta_{h-max}/H) \%_{(for\ \mu=1)} \tag{1}$$

$$\delta_{v-fric} \% = (\delta_{v-max}/H) \%_{(for\ any\ \mu\ value)} - (\delta_{v-max}/H) \%_{(for\ \mu=1)} \tag{2}$$

These factors give the percentage increase of δ_{h-max} (or δ_{v-max}) for any μ value from that at $\mu = 1$. Figure 8 shows that this increase of δ_{h-fric} is the highest at $\mu = 0$ of 0.19% at $H = 6$ m and decreases to 0.01% at $H = 3$ m. $\delta_{h-fric} \%$ value at $\mu = 0.1$ drops to about 0.07% for $H = 6$ m while it keeps almost constant at 0.01% for $H = 3$ m. As μ value increases $\delta_{h-fric} \%$ decreases. $\delta_{h-fric} \%$ becomes insignificant at $\mu = 0.67$ where all $\delta_{h-fric} \%$ values are $\leq 0.01\%$. Similar trend was found for maximum vertical displacement ratio of soil adjacent to the excavation, $\delta_{v-fric} \%$.

Figure 6 shows $\delta_h/H\%$ distribution along pile wall width at the top of the wall for HS, HF, and HH cases, respectively, for small value of $\mu = 0.1$ and perfect bonding of $\mu = 1$, where each point of the curve represents $\delta_h/H\%$ at the pile head. $\delta_h/H\%$ of the edge piles for HF and HS cases are almost the same

Fig. 8 Variation of $\delta_{h-fric} \%$ at different μ values ($D_r = 50\%$, $L = 20$ m)



or very close to HH case, respectively, for all μ values. However, the difference increases by moving toward the middle of the pile wall. $\delta_h/H\%$ increases significantly at the pile wall middle as $E_p I_p$ increases from HS to HF to HH cases. The situation becomes worse for $\mu = 0.1$, where weak bonding between piles. The difference in $\delta_h/H\%$ becomes larger as the difference between E_p for the two adjacent piles increases, as shown in Fig. 6. Figure 7 presents $M_{\max} L_p/E_p I_p$ variation along pile wall width for different values of μ for cases of HS, HF, and HH. The discontinuity of bending moment for HS and HF is clearer than the cases of $\delta_h/H\%$. As bonding between piles increases the discontinuity disappear gradually. However, for HH cases, there is a continuity in bending moment between piles for all cases regardless of μ values as all piles have the same flexural stiffness.

Discussion

From the present study, it is found that there are four main parameters that control the behavior of cantilever pile wall in supporting excavation in sand. These parameters are sand relative density (D_r), excavation depth (H), wall flexural stiffness factor ($E_p I_p/L_p$), and the bonding between piles in the wall (μ). The common design technique is to limit the maximum lateral wall deflection. Different design methods were proposed (Rowe 1952; Clough and O'Rourke 1990; Addenbrooke 1994; Bryson and Zapata-Medina 2012) based on the wall flexibility. However, they focus mainly on braced deep excavation in clayey soil. Cantilever pile walls in sandy soil has almost limited proposed design method although the widespread use of such wall types for shallow excavation. According to Poulos and Davis (1980), the relative stiffness of laterally loaded rigid and flexible piles to that of the soil (K_r) can be rewritten as follows:

$$K_r = \frac{EI}{E_s D^4} \tag{3}$$

where D is the embedded length of the pile. For K_r larger than 0.01, the pile is considered as a rigid pile wall.

The results of the present study will be used to propose a design method to design cantilever pile wall to support excavation in sand. The first case in this design method is the fully bonded pile wall case ($\mu = 1$). While the second case is for the partially bonded or un-bonded pile walls for all HS, HF, and HH cases. So, one can calculate the predicted $\delta_{h-\max}/H\%$ or $\delta_{v-\max}/H\%$ for fully bonded pile wall and then can calculate the increase of the deformation due to partially bonded or un-bonded pile wall cases.

Proposed design method for fully bonded pile wall

All cases of fully bonded pile wall ($\mu = 1$) are analyzed to propose an expression that can be used to predict the maximum lateral deflection of pile wall ($\delta_{h-\max}$) and the maximum vertical displacement of the ground surface adjacent to the excavation ($\delta_{v-\max}$). In this analysis, sand relative density (D_r) and the embedded length of the pile wall (D) have been considered as variable parameters for all cases of HS, HF, and HH pile wall. It should be noted that this proposed design method is based on data of $L = 20$ m. As the effect of pile wall length is negligible for flexible pile wall ($K_r < 0.01$), the design method is still applicable for the other wall lengths considering $K_r < 0.01$. Figure 5 shows the relationship between $\delta_{h-\max}/H\%$, D_r and H for HS, HF, and HH pile wall cases. The results of the parametric study were fitted as shown in Fig. 5 for all cases HS, HF, and HH. It was found that $\delta_{h-\max}/H\%$ can be calculated using the following equation:

$$\delta_{h-\max}/H\% = \frac{(H-1.96)}{B + (C * D_r^2)} \tag{4.a}$$

where B and C are constants that can be calculated as a function of (EI_p^*/EI_{p-HH}) ; where EI_p^* is the average flexural stiffness of the pile wall, and EI_{p-HH} is the flexural stiffness of the pile wall of hard piles (considering the hard pile is RC pile of $E = 2.1 \times 10^7$ kN/m², and wall thickness is 0.5 m). These constants can be calculated as follows:

$$B = 3.28 \ln(EI_p^*/EI_{p-HH}) + 6.52 \tag{4.b}$$

$$C = 0.0011 \ln(EI_p^*/EI_{p-HH}) + 0.0022 \tag{4.c}$$

In the same way, $\delta_{v-\max}$ can be predicted. It was found that $\delta_{v-\max}/H\%$ can be calculated using the following equation:

$$\delta_{v-\max}/H\% = \frac{(H-2.36)}{B + (C * D_r^2)} \tag{5.a}$$

where B and C are constants that can be calculated as a function of (EI_p^*/EI_{p-HH}) . They can be calculated as follows:

$$B = -27.2 \left(EI_p^*/EI_{p-HH} \right)^2 + 48.6 \left(EI_p^*/EI_{p-HH} \right) - 15.45 \tag{5.b}$$

$$C = 0.0044 \left(EI_p^*/EI_{p-HH} \right)^2 - 0.0057 \left(EI_p^*/EI_{p-HH} \right) + 0.0041 \tag{5.c}$$

Proposed design method for partially bonded or un-bonded pile wall

To consider the bonding coefficient μ in the analysis, the excavation depth (H) parameter has been combined with D_r (where elastic modulus of soil is a function of D_r , as discussed before, see Table 1) and E_p in the relative stiffness factor K_r . So, both μ and K_r are considered as variable parameters to calculate $\delta_{h-fric.}\%$ or $\delta_{v-fric.}\%$. Such relationships for $\delta_{h-fric.}\%$ are shown in Fig. 9 and can be calculated as follows:

$$\delta_{h-fric.}\% = \frac{A + (B * K_r)}{1 + (C * \mu) + 18.1\mu^2} \tag{6.a}$$

where A , B , and C are constants that can be calculated as a function of D_r and EI_p^*/EI_{p-HH} ratio:

$$A = \frac{D_r - 176.7}{39.74 + 837 \left(\frac{EI_p^*}{EI_{p-HH}} \right)} \tag{6.b}$$

$$B = \exp \left(8.54 - \frac{19.54}{D_r} - 1.93 \text{Log} \left(\frac{EI_p^*}{EI_{p-HH}} \right) \right) \tag{6.c}$$

$$C = 0.124 + 5.75 \left(\frac{EI_p^*}{EI_{p-HH}} \right) + \frac{342.2}{D_r} \tag{6.d}$$

In the same way $\delta_{v-fric.}\%$ can be predicted as a function of the bonding coefficient μ and the relative stiffness factor K_r . It can be calculated as follows:

$$\delta_{v-fric.}\% = \frac{A + (B * K_r)}{1 + (C * \mu) + 17.85\mu^2} \tag{7.a}$$

where A , B , and C are constants that can be calculated as a function of D_r and E_p^*/E_{p-HH} ratio:

$$A = \frac{D_r - 144.5}{11.1 + 645.5 \left(\frac{EI_p^*}{EI_{p-HH}} \right)} \tag{7.b}$$

$$B = \exp \left(8.24 - \frac{5.5}{D_r} - 1.95 \text{Log} \left(\frac{EI_p^*}{EI_{p-HH}} \right) \right) \tag{7.c}$$

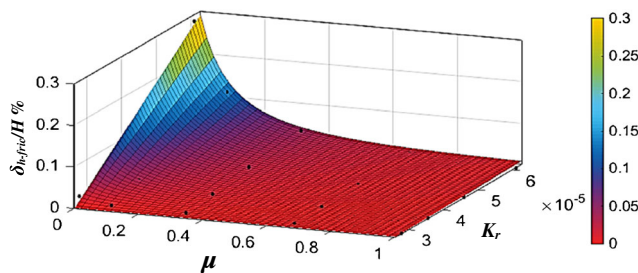


Fig. 9 Variation of $\delta_{h-fric.}/H\%$ for partially or un-bonded pile wall for HS cases ($D_r = 50\%$ and $L = 20$ m)

$$C = 6.66 + \left(\frac{338.7}{D_r} \right) - \frac{1.1}{\left(\frac{EI_p^*}{EI_{p-HH}} \right)^2} \tag{7.d}$$

Illustrative example

If we assume a CSPW of 15 m length embedded in sandy soil of 60% relative density, the excavation depth is 4 m, and the wall is constructed of H-F system, $\delta_{h-max}/H\%$ and $\delta_{v-max}/H\%$ can be predicted using equations (4) and (5), respectively. First, both the constants B and C can be calculated as a function of EI_p^*/EI_{p-HH} ratio using equations (4-b) and (4-c), respectively, for $\delta_{h-max}/H\%$ calculations. For $\delta_{v-max}/H\%$ calculations, constants B and C can be calculated using equations (5-b) and (5-c) as a function of EI_p^*/EI_{p-HH} ratio. It should be noted that EI_{p-HH} equals to 218,750 kN m²/m considering the hard pile is RC pile of $E = 2.1 \times 10^7$ kN/m², and wall thickness is 0.5 m. Then, $\delta_{h-max}/H\%$ and $\delta_{v-max}/H\%$ can be calculated using both equations (4-a) and (5-a), respectively. Following these steps, $\delta_{h-max}/H\% = 0.16\%$ and $\delta_{v-max}/H\% = 0.114\%$ which are corresponding to $\delta_{h-max} = 6.43$ mm and $\delta_{v-max} = 4.55$ mm, respectively.

In case that bonding coefficient between piles μ is known, the increase in $\delta_{h-max}/H\%$ and $\delta_{v-max}/H\%$ can be calculated as $\delta_{h-fric.}\%$ and $\delta_{v-fric.}\%$, respectively. If μ is unknown or for any unexpected construction problems, it can be assumed that no bonding between piles (tangent piles) and the calculated $\delta_{h-fric.}\%$ and $\delta_{v-fric.}\%$ will be the upper limit case. So, assuming $\mu = 0$, $\delta_{h-fric.}\%$ can be obtained by calculating constants A , B , and C using equations (6-b), (6-c), and (6-d), respectively. Following these steps, $\delta_{h-fric.}\%$ for the current example will be equal to 0.147%. This means that δ_{h-max} for no bonding case (tangent piles) will be 12.3 mm. Similarly, $\delta_{v-fric.}\%$ can be obtained using equation (7). $\delta_{v-fric.}\%$ will be equal to 0.132% and δ_{v-max} will be equal to 9.82 mm. This means that both δ_{h-max} and δ_{v-max} have been increased twice when the piles within the wall have no bonding between them. It should be noted that all equations were derived for the case of $L = 20$ m. As the effect of wall length is insignificant as discussed before, so $L = 20$ m should be used in the calculations of K_r .

Conclusion

The present research studies the behavior of cantilever secant pile wall (SPW) in supporting excavation in sandy soil. A parametric study of a wide range of sand relative density (D_r), excavation depth (H), wall length (L_p), wall flexural stiffness ($E_p I_p$), and bonding between piles within the wall (μ) has been carried out. The following conclusion can be derived:

1. It is found that increasing D_r , H , and $E_p I_p / L_p$ will decrease both δ_h and δ_v .
2. An excavation depth (H) of ≤ 2 m is recommended for the cantilever stage before installing the first support of the wall (strut or anchor). At such excavation depth, soil deformation is not significant in sandy soil.
3. A design method has been proposed that allows to predict both $\delta_{h-\max}$ and $\delta_{v-\max}$ according to those three parameters (D_r , H , $E_p I_p$) for fully bonded piles.
4. The effect of bonding between piles within the wall has been examined. It can be concluded that such parameter is highly significant in changing both $\delta_{h-\max}$ and $\delta_{v-\max}$.
5. A design method has been proposed to predict the increase of $\delta_{h-\max}$ and $\delta_{v-\max}$ according to the friction coefficient (μ) between piles as a function of wall relative stiffness (K_r), sand relative density (D_r), and wall stiffness.
6. It was found that $\mu < 0.33$ is highly significant in increasing both δ_h and δ_v .
7. Such design method can be used with limitation to the range of the parameters (D_r , H , $E_p I_p$) that have been used in the present analysis.

It is recommended for future studies to come up with a formula or a model that can predict the value of friction coefficient between piles according to different construction conditions; e.g., time intervals of bonding (TIB), and the primary pile compressive strength at the time of installing the secondary pile.

Funding information This work was supported by the Deanship of Scientific Research (DSR), King Abdulaziz University, Jeddah, under grant no. (829-128-D1436). The authors, therefore, gratefully acknowledge the DSR technical and financial support.

References

- Achmus M, Thieken K, Saathoff J, Terceros M, Albiker J (2019) Un- and reloading stiffness of monopile foundations in sand. *Applied Ocean Research*. 84:62–73. <https://doi.org/10.1016/j.apor.2019.01.001>
- Addenbrooke TI (1994) A flexibility number for the displacement controlled design of multi propped retaining walls. *Journal of Ground Engineering*. 27(7):41–45
- Altuntas, C., Persaud, D., and Poeppel, A. R. (2009) Secant pile wall design and construction in Manhattan. Proc., Int. Foundation Congress and Equipment Expo (IFCEE2009), ASCE, Reston, VA, 105–112.
- Bica AVD, Clayton CRI (1989) Limit equilibrium design methods for free embedded cantilever walls in granular materials. *Proc. Instn Civ. Engrs Part 1* 86. No. 5:879–989
- Bica A, Clayton C (2004) An experimental study of the behaviour of embedded lengths of cantilever walls. *Géotechnique*. 48(6):731–745. <https://doi.org/10.1680/geot.1998.48.6.731>
- Bolton MD (1986) The strength and dilatancy of sands. *Géotechnique* 36(1):65–78
- Bolton MD, Powrie W (1987) Collapse of diaphragm walls retaining clay. *Géotechnique*, 37. No. 3:335–353. <https://doi.org/10.1680/geot.1987.37.3.335>
- Bolton MD, Powrie W, Symons IF (1989) The design of stiff in-situ walls retaining overconsolidated clay, part I – short term behaviour. *Ground Engng* 22(8/9):34–47
- Bolton MD, Powrie W, Symons IF (1990) The design of stiff in-situ walls retaining overconsolidated clay, part II – long term behaviour. *Ground Engng* 23. No. 2:22–28
- Brinkgreve R, Engin E, Engin H (2010) Validation of empirical formulas to derive model parameters for sands. In: Brinkgreve R, Engin E, Engin H (eds) 7th International Conference of Numerical Methods in Geotechnical Engineering. Trondheim, Norway. <https://doi.org/10.1201/b10551-25>
- Bryson LS, Medina DG (2010) Finite element analyses of secant pile wall installation. *Proc Inst Civ Eng, Geotech Eng* 163(4):209–219
- Bryson LS, Zapata-Medina DG (2012) Method for estimating system stiffness for excavation support walls. *Journal of Geotechnical and Geoenvironmental Engineering*. 138(9):1104–1115. [https://doi.org/10.1061/\(ASCE\)GT.1943-5606.0000683](https://doi.org/10.1061/(ASCE)GT.1943-5606.0000683)
- Burland JB, Potts DM, Walsh NM (1981) The overall stability of free and propped embedded cantilever retaining walls. *Ground Engineering*, 14. No. 5:28–37
- Clough GW, O'Rourke T (1990) Construction induced movements of in situ walls. *Proceedings of Design and performance of Earth Retaining Structures*, ASCE Special Conference, Ithaca, New York, pp 439–470
- Conte E, Troncone A, Vena M (2013) Nonlinear three-dimensional analysis of reinforced concrete piles subjected to horizontal loading. *Comput. Geotech.* 49:123–133
- Conte E, Troncone A, Vena M (2015) Behaviour of flexible piles subjected to inclined loads. *Comput. Geotech.* 69:199–209
- Conte E, Troncone A, Vena M (2017) A method for the design of embedded cantilever retaining walls under static and seismic loading. *Géotechnique* 67(12):1081–1089
- Day RA (2001) Earth pressure on cantilever walls at design retained heights. *Proc. Instn Civ. Engrs Geotech. Engng* 149. No. 3:167–176
- Dong YP, Burd HJ, Houlsby GT (2012) 3D FEM modelling of a deep excavation case history considering small-strain stiffness of soil and thermal contraction of concrete. In: *Proceedings of the BGA Young Geotechnical Engineers's Symposium*. University of Leeds, Leeds, UK
- Dong Y, Burd H, Houlsby G (2014) Advanced finite element analysis of a complex deep excavation case history in Shanghai. *Front. Struct. Civ. Eng.* 8:93–100. <https://doi.org/10.1007/s11709-014-0232-3>
- Finno RJ, Bryson S (2002) Response of building adjacent to stiff excavation support system in soft clay. *Journal of Performance of Constructed Facilities*. 16(1):10–20. [https://doi.org/10.1061/\(ASCE\)0887-3828\(2002\)16:1\(10](https://doi.org/10.1061/(ASCE)0887-3828(2002)16:1(10)
- Finno RJ, Bryson S, Calvello M (2002) Performance of a stiff support system in soft clay. *J Geotech Geoenviron Eng* 128(8):660–671. [https://doi.org/10.1061/\(ASCE\)1090-0241\(2002\)128:8\(660](https://doi.org/10.1061/(ASCE)1090-0241(2002)128:8(660)
- Finno RJ, Tanner BJ, Roboski JF (2006) Three-dimensional effects for supported excavations in clay. *Journal of Geotechnical and Geoenvironmental Engineering*. 133(1). [https://doi.org/10.1061/\(ASCE\)1090-0241\(2007\)133:1\(30](https://doi.org/10.1061/(ASCE)1090-0241(2007)133:1(30)
- Gannon J (2016) Primary firm secant pile concrete specification. *Proceedings of the Institution of Civil Engineers - Geotechnical Engineering* 169(2):110–120. <https://doi.org/10.1680/jgeen.15.00038>
- Gaudin C, Garnier J, Thorel L (2004) Physical modelling of a cantilever wall. *International Journal of Physical Modelling in Geotechnics* 4(2):13–26
- Gazetas G, Garini E, Zafeirakos A (2016) Seismic analysis of tall anchored sheet-pile walls. *Soil Dynamics and Earthquake*

- Engineering. 91:209–221. <https://doi.org/10.1016/j.soildyn.2016.09.031>
- Ge X (2002) Response of a shield-driven tunnel to deep excavations in soft clay. PhD Thesis, Hong Kong University of Science and Technology.
- Hashash Y (1992) Analysis of deep excavations in clay. Ph. D. Thesis, Massachusetts Institute of Technology, Dept. of Civil Engineering.
- Hikooei BF (2013) Numerical modeling of pipe-soil interaction under transverse direction. Master's thesis, University of Calgary, Calgary – Alberta, Canada
- Hsiung B (2009) A case study on the behaviour of a deep excavation in sand. *Computers and Geotechnics*. 36(4):665–675. <https://doi.org/10.1016/j.compgeo.2008.10.003>
- Hsiung B, Yang K, Aila W, Hung C (2016) Three-dimensional effects of a deep excavation on wall deflections in loose to medium dense sands. *Computers and Geotechnics*. 80:138–151. <https://doi.org/10.1016/j.compgeo.2016.07.001>
- Hu ZF, Yue ZQ, Zhou J, Tham LG (2003) Design and construction of a deep excavation in soft soils adjacent to the Shanghai Metro tunnels. *Canadian Geotechnical Journal*. 40(5):933–948. <https://doi.org/10.1139/t03-041>
- Jefferies M, Been K (2006) Soil liquefaction: a critical state approach. Taylor & Francis, Abingdon, UK
- Ji X, Ni P, Zhao W, Yu H (2019) Top-down excavation of an underpass linking two large-scale basements in sandy soil. *Arabian Journal for Geosciences* 12:314. <https://doi.org/10.1007/s12517-019-4493-y>
- Kenny S, Jukes P (2015) Pipeline/soil interaction modeling in support of pipeline engineering design and integrity. In: *Oil and Gas Pipelines: Integrity and Safety Handbook*, pp 99–142
- Khoiri M, Ou C (2013) Evaluation of deformation parameter for deep excavation in sand through case histories. *Computers and Geotechnics*. 47:57–67. <https://doi.org/10.1016/j.compgeo.2012.06.009>
- King GJW (1995) Analysis of cantilever sheet-pile walls in cohesionless soil. *J. Geotech. Engng, ASCE* 121(9):629–635
- King G, McLoughlin J (1993) Centrifuge model studies of a cantilever retaining wall in sand. *Retaining structures*. ICE:711–720
- Knappett J, Caucis K, Brown M, Jeffrey J, Ball J (2016) CHD pile performance: part II – numerical modelling. *Proceedings of the Institution of Civil Engineers - Geotechnical Engineering*. 169(5): 436–454. <https://doi.org/10.1680/jgeen.15.00132>
- Korff, M., Tol, A.F. van & Jong, E. de (2007) Risks related to CFA-pile walls. 14th European Conference on Soils (Mechanics and Geotechnical Engineering), Madrid - Spain.
- Kung GT, Juang C, Hsiao E, Hashash Y (2007) Simplified model for wall deflection and ground-surface settlement caused by braced excavation in clays. *Journal of Geotechnical and Geoenvironmental Engineering*. 133(6):731–747. [https://doi.org/10.1061/\(ASCE\)1090-0241\(2007\)133:6\(731](https://doi.org/10.1061/(ASCE)1090-0241(2007)133:6(731)
- Li AZ, Lehane BM (2010) Embedded cantilever retaining walls in sand. *Géotechnique*. 60(11):813–823. <https://doi.org/10.1680/geot.8.P.147>
- Liao S-M, Li W-L, Fan Y-Y, Sun X, Shi Z-H (2014) Model test on lateral loading performance of secant pile walls. *Journal of Performance of Constructed Facilities*. 28(2):391–401. [https://doi.org/10.1061/\(ASCE\)CF.1943-5509.0000374](https://doi.org/10.1061/(ASCE)CF.1943-5509.0000374)
- Liu GB, Ng CW, Wang ZW (2005) Observed performance of a deep multistrutted excavation in Shanghai soft clays. *Journal of Geotechnical and Geoenvironmental Engineering*. 131(8):1004–1013. [https://doi.org/10.1061/\(ASCE\)1090-0241\(2005\)131:8\(1004](https://doi.org/10.1061/(ASCE)1090-0241(2005)131:8(1004)
- Liu G, Jiang R, Ng C, Hong Y (2011) Deformation characteristics of a 38 m deep excavation in soft clay. *Canadian Geotechnical Journal*. 48(12):1817–1828. <https://doi.org/10.1139/t11-075>
- Liu N, Duan N, Yu F (2018) Deformation characteristics of retaining structures and nearby buildings for different propped retaining walls in soft soil. *Journal of Testing and Evaluation*. 47(3):1829–1847. <https://doi.org/10.1520/JTE20170763>
- Long M (2001) Database for retaining wall and ground movements due to deep excavation. *Journal of Geotechnical and Geoenvironmental Engineering*. 127(3):203–224. [https://doi.org/10.1061/\(ASCE\)1090-0241\(2001\)127:3\(203](https://doi.org/10.1061/(ASCE)1090-0241(2001)127:3(203)
- Madabhushi G, Chandrasekaran VS (2005) Rotation of cantilever sheet pile walls. *J Geotech Geoenviron. Eng* 131:202–212
- Madabhushi SPG, Zeng X (2006) Seismic response of flexible cantilever retaining walls with dry backfill. *Geomech. Geoenngng* 1. No. 4: 275–289
- Martinkus V, Norkus A, Mikolainis M (2017) Numerical simulation of displacement model pile test performed in artificial sand deposit. *Procedia Engineering*. 172:715–722. <https://doi.org/10.1016/j.proeng.2017.02.091>
- Mei GX, Chen QM, Song LH (2009) Model for predicting displacement-dependent lateral earth pressure. *Can. Geotech. J.* 46(8):969–975
- Milligan G, St John H, O'Rourke H (2008) Contributions to Géotechnique 1948–2008: Retaining structures. *Géotechnique*. 58(5):377–383. <https://doi.org/10.1680/geot.2008.58.5.377>
- Mohamad H, Soga K, Pellevé A, Bennett P (2011) Performance monitoring of a secant-piled wall using distributed fiber optic strain sensing. *J Geotech Geoenviron Eng* 137(12). [https://doi.org/10.1061/\(ASCE\)GT.1943-5606.0000543](https://doi.org/10.1061/(ASCE)GT.1943-5606.0000543)
- Moormann C (2004) Analysis of wall and ground movements due to deep excavations in soft soil based on a new worldwide database. *Soils And Foundations*. 44(1):87–98. <https://doi.org/10.3208/sandf.44.87>
- Ng C, Hong Y, Liu G, Liu T (2012) Ground deformations and soil-structure interaction of a multi-propped excavation in Shanghai soft clays. *Géotechnique*. 62(10):907–921. <https://doi.org/10.1680/geot.10.P.072>
- Ng CWW, Shi J, Mašin D, Sun H, Lei GH (2015) Influence of sand density and retaining wall stiffness on three-dimensional responses of tunnel to basement excavation. *Can. Geotech. J.* 52(11):1811–1829. <https://doi.org/10.1139/cgj-2014-0150>
- Nie D (2019) Analysis on the effect of excavation by sections for large foundation pit without horizontal struts. In: *International Symposium for Intelligent Transportation and Smart City (ITASC) 2019 Proceedings*. ITASC 2019. Smart Innovation, Systems and Technologies, vol 127. Springer, Singapore
- Nikolinakou M, Whittle A, Savidis S, Schran U (2011) Prediction and interpretation of the performance of a deep excavation in Berlin sand. *Journal of Geotechnical and Geoenvironmental Engineering*. 137(11):1047–1061. [https://doi.org/10.1061/\(ASCE\)GT.1943-5606.0000518](https://doi.org/10.1061/(ASCE)GT.1943-5606.0000518)
- Osouli A, Hashash Y (2010) Case studies of prediction of excavation response using learned excavation performance. *International Journal of Geoenvironment Case Histories*. 1(4):340–366
- Ou CY (2006) Deep excavation: theory and practice. Taylor & Francis, Netherlands
- Ou C, Hsieh P, Chiou D (1993) Characteristics of ground surface settlement during excavation. *Canadian Geotechnical Journal* 30(5):758–767. <https://doi.org/10.1139/t93-068>
- Ou C-Y, Hsieh P-G, Chiou D-C (2010) Characteristics of ground surface settlement during excavation. *Canadian Geotechnical Journal*. 30(5):758–767. <https://doi.org/10.1139/t93-068>
- Panagoulas S, Hosseini S, Brinkgreve R (2018) An innovative design methodology for offshore wind monopile foundations. 26th European Young Geotechnical Engineers Conference, Graz, Austria.
- PLAXIS 3D FOUNDATION (2006) Version 1.5 PLAXIS finite element code for soil and rock analysis. Delft University of Technology & PLAXIS B. V, Delft.
- Poulos HG, Davis EH (1980) Pile foundation analysis and design. Wiley, New York

- Ramadan MI, Ramadan EH, Khashila MM (2018) Cantilever contiguous pile wall for supporting excavation in clay. *Geotechnical and Geological Engineering Journal*. 36:1545–1558. <https://doi.org/10.1007/s10706-017-0407-5>
- Rowe P (1952) Anchored sheet pile walls. *Proc Inst Civ Eng* 1(1):27–70 (PART 1)
- Rowe PW, Peaker K (1965) Passive earth pressure measurements. *Geotechnique* 15(1):57–78
- Sert S, Luo Z, Xiao J, Gong W, Juang C (2016) Probabilistic analysis of responses of cantilever wall-supported excavations in sands considering vertical spatial variability. *Computers and Geotechnics*. 75: 182–191. <https://doi.org/10.1016/j.compgeo.2016.02.004>
- Tan Y, Wei B (2011) Observed behaviors of a long and deep excavation constructed by cut-and-cover technique in Shanghai soft clay. *Journal of Geotechnical and Geoenvironmental Engineering*. 138(1):69–88. [https://doi.org/10.1061/\(ASCE\)GT.1943-5606.0000553](https://doi.org/10.1061/(ASCE)GT.1943-5606.0000553)
- Turner J, Steele J, Maher W, Zortman M, Carpenter J (2004) Design, construction, and performance of an anchored tangent pile wall for excavation support. *GeoSupport 2004*, ASCE:322–333
- Wong IH, Poh TY, Chuah HL (2002) Performance of excavations for depressed expressway in Singapore. *Journal of Geotechnical and Geoenvironmental Engineering*. 123(7). [https://doi.org/10.1061/\(ASCE\)1090-0241\(1997\)123:7\(617](https://doi.org/10.1061/(ASCE)1090-0241(1997)123:7(617)
- Zahmatkesh A, Choobbasti AJ (2015) Evaluation of wall deflections and ground surface settlements in deep excavations. *Arabian Journal of Geosciences*. 8(5):3055–3063. <https://doi.org/10.1007/s12517-014-1419-6>
- Zdravkovic L, Potts DM, St. John HD (2005) Modelling of a 3D excavation in finite element analysis. *Geotechnique* 55(7):497–513
- Zhu W, Yi J (1988) Application of centrifuge modelling to study a failed quay wall. In: *Proceedings International Conference Centrifuge 88*, Paris: 415–419